DR. SLOBODAN CUK, President, TESLAco

Single-Stage Isolated Bridgeless PFC Converter Achieves 98% Efficiency

A Single-stage Isolated Bridgeless PFC Converter (patents pending) has a single isolation transformer, three switches, and 98% efficiency compared to four magnetic pieces, 14 switches, and 89% efficiency of the conventional Three-stage approach. It achieves best in-class PFC performance with 0.999 power factor and 1.7% total harmonic distortion.

Another Isolated Bridgeless PFC converter (patents pending) with pulsating input current and based on a novel Hybrid-switching method eliminates the front-end full-bridge rectifier, yet provides isolation in a Single-stage power processing, resulting in performance, size, and cost advantages over conventional Three- stage, bridge-type PFC converters.

The single-stage isolated bridgeless PFC Converter with pulsating input current attains improved efficiency of over 98% (achievable with appropriate switching devices) compared to 89% of the Three-stage approach, offering simultaneously significant size and cost reductions, while maintaining the near unity power factor of 0.999 and 1.7% total harmonic distortion. The single-stage converter uses just a single magnetic part (the isolation transformer) and three switches, compared with compared to four magnetic pieces and 14-switches of the conventional Three-stage approach. This pulsating version requires only a single resonant capacitor and no input inductor, when compared to the Isolated Bridgeless Converter presented in October 2010 issue of *Power Electronics Technology*.

The new non-isolated Bridgeless PFC converter with pulsating input current of Fig. 1a operates directly of the ac line and without the need for a Full-Bridge rectifier in front. Despite the use of a resonant inductor and a resonant capacitor, thanks to the novel hybrid-switching method, the DC voltage gain depends on the duty ratio only and NOT on resonant component values or the load current. Furthermore, the converter's DC voltage gain is the same for either positive input voltage or negative input voltage. Hence, it provides automatic ac line rectification, without the need for a bridge rectifier.

Although the converter topology resembles that of conventional flyback converter, its voltage gain characteristics in the operating step-up region is entirely different and not the flyback converter type with DC voltage gain of D/ (1-D), but instead of the boost converter type with DC voltage gain 1/(1-D).

The isolated version of the converter is obtained simply

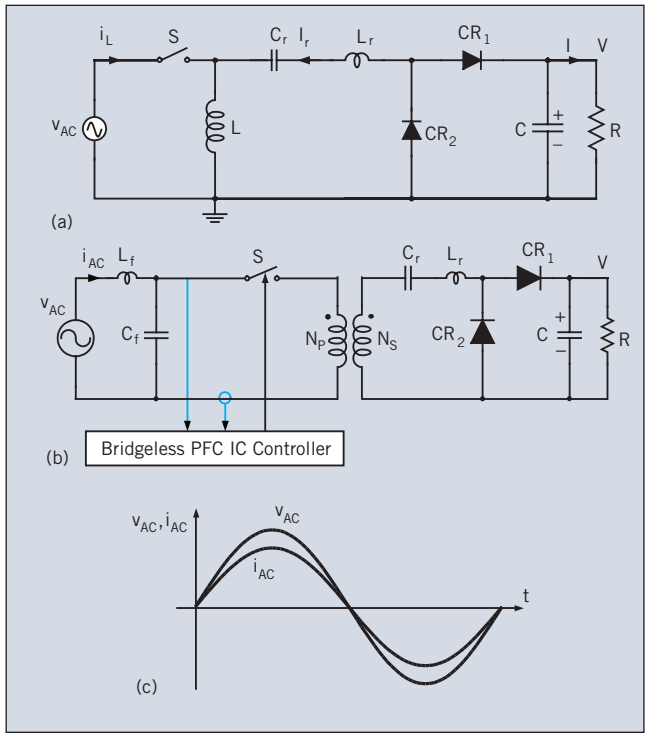

Fig. 1(a) Operating directly from the ac line, this converter operates is the second true single-stage bridgeless ac-dc converter with PFC. It has one controlling switch and two diode switches, and in addition to a PWM inductor a small resonant inductor and small resonant capacitor. (b) The new Isolated Bridgeless PFC converter and Bridgeless PFC IC controller operates by sensing directly the full-wave AC line voltage and AC line currents and controlling switch S. (c) The switch S is controlled by the Bridgeless PFC IC controller, so as to force the line current to be proportional to the sinusoidal line voltage and in phase with it.

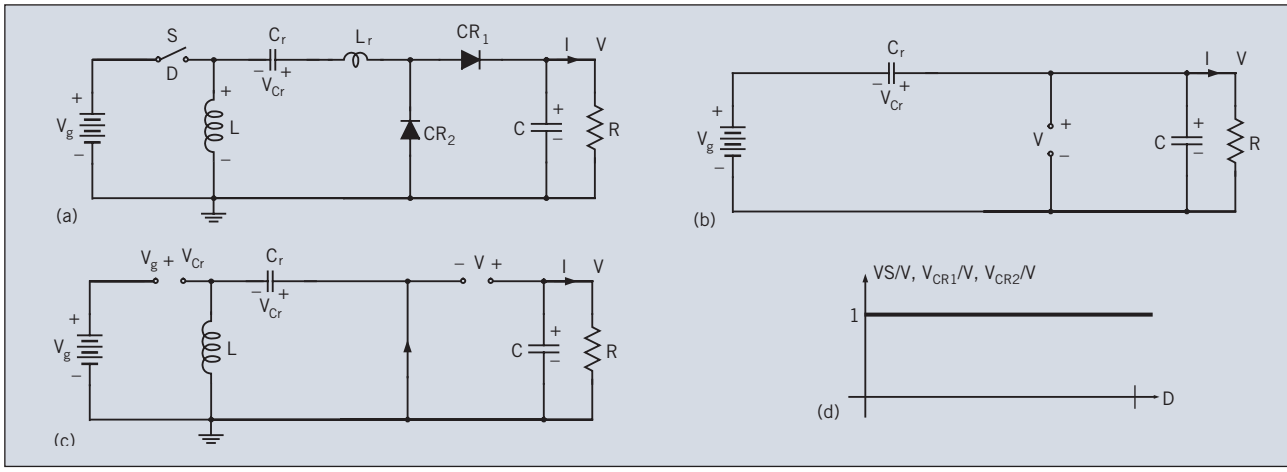

Fig. 2 (a) Shows the operation from a positive half-cycle of sinusoidal ac line voltage is shown by this DC-DC converter. (b) The equivalent circuit model for ON-time interval. (c) The equivalent circuit model for the OFF-time interval. (d) The voltage stresses of three switches.

by replacing replacing a single inductance L in converter of *Fig. 1a* with a two-winding isolation transformer with NP:NS turns ratio, as illustrated in the Single-Stage Isolated Bridgeless PFC converter *Fig. 1b*. The duty ratio control of the power stage with the help of Bridgeless PFC IC Controller and high frequency input filter shown in Fig. 1b results in clean sinusoidal input current drawn in phase with sinusoidal input line voltage and proportional to it, resulting in unity power factor. The measured power factor on experimental 400W prototype was 0.999 for 110V ac, 60Hz line.

BRIDGELESS PFC CONVERTER OPERATION

A very clear objective to increase the efficiency is to devise a converter, which can eliminate a front-end full-bridge rectifier. Past attempts failed to eliminate diode-bridge rectifiers, leading to the belief that the solution to such a goal may be "impossible" and that such converter topology could not exist. This is shown to be no longer the case as the July and August issues of *Power Electronics Technology* demonstrated a non-isolated True Bridgeless PFC converter and the October issue introduced an Isolated Bridgeless PFC converter based on it. Here, another True Bridgeless PFC converter topology (non-isolated and isolated ones) is introduced which is even simpler, such as the pulsating input current converter topology of *Fig. 1a*.

This converter topology comprises only three switches: one controllable switch S and two passive current rectifier switches CR1 and CR2 as seen in *Fig. 1a*, which turn-ON and turn-OFF in response to the state of the main controlling switch S for either positive or negative polarity of the input ac voltage.

Thus, switch S alone controls both diode switches, whose states are changed automatically according to the polarity of

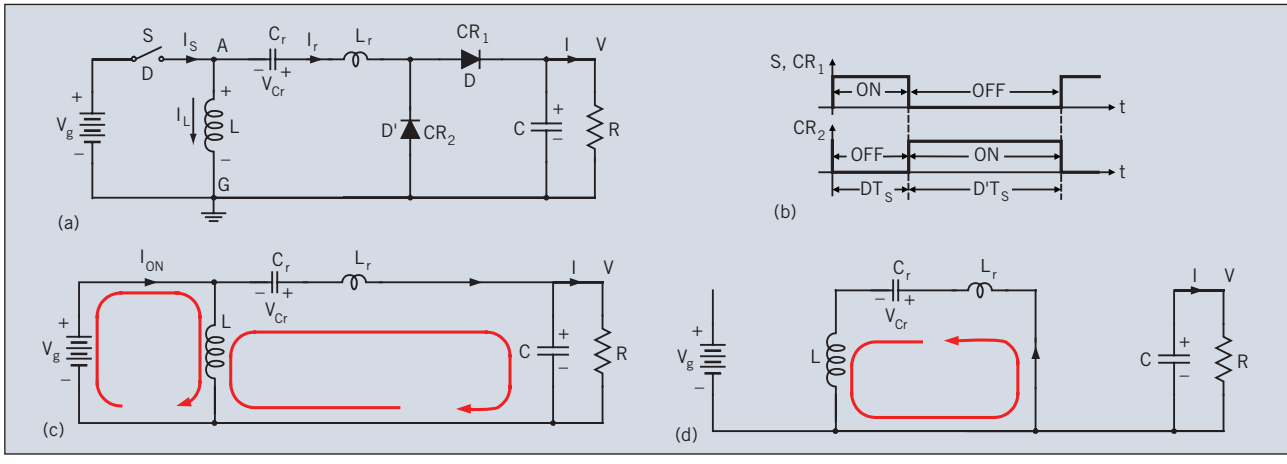

Fig. 3. Bridgeless PFC converter operation for positive half-cycle of input voltage. (a) Switch S operates in phase with diode CR1 and out of phase with diode CR2. (b) States of the switches of PFC converter (c) Linear switched networks for ON-time interval (d) Linear switched network for OFF-time interval

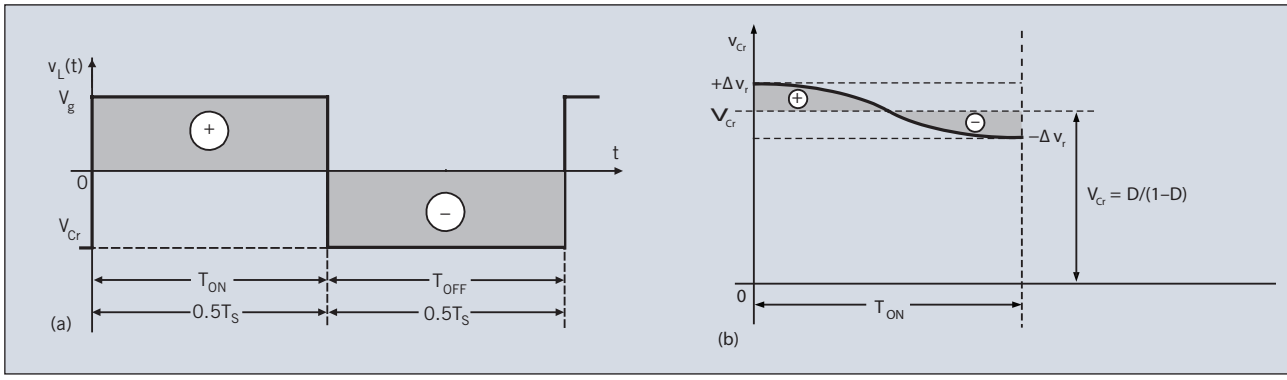

Fig. 4. PWM inductor L is excited as in PWM converters with a square-wave like voltage over entire switching period while resonant inductor is excited over the ON-time interval only: (a) Voltage waveform of the PWM inductor and respective positive flux excursions (shaded area designated with positive sign) and negative flux excursions (shaded area designated with negative sign. (b) Resonant inductor Lr is excited with a co-sinusoidal ac ripple voltage Δvr of the resonant capacitor Cr and is fully flux-balanced during only ON-time interval (see respective shaded areas).

the ac input voltage. For example, for the positive polarity of the ac input voltage, current rectifier CR1 conducts during the ON-time interval of switch S. Then, for negative polarity of ac input voltage, the same current rectifier CR1 conducts during the OFF-time interval of switch S. The current rectifier CR2 also responds automatically to the state of the switch S and polarity of the input ac voltage. For the positive polarity it conducts during the OFF-time interval of switch S and for negative polarity, it conducts during the ON-time interval of switch S.

Thus, the three switches operate at all times, for both positive and negative half-cycles of the input ac line voltage.

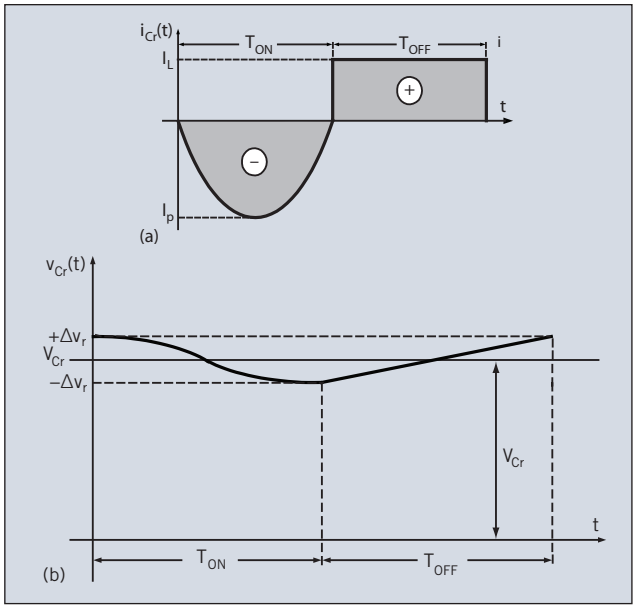

Fig. 5. Resonant inductor current and resonant capacitor voltage waveforms during the entire switching period (a) Resonant inductor current ir during entire switching period (b) Resonant capacitor voltage shows the linear charging of the resonant capacitor Cr during the OFF-time interval.

Hence, this true Bridgeless PFC converter™ operates without the full-bridge rectifier, since the converter topology itself performs an implied ac line rectification to result in DC output voltage for either polarity of input ac line voltage. Eliminating the full-bridge rectifier directly eliminates large losses, especially for the low line of 85V.

As seen in *Fig. 1a*, this topology also consists of the floating energy transferring capacitor Cr, which acts as a resonant capacitor for the part of the switching cycle, and a resonant inductor Lr and an isolation transformer.

VOLTAGE STRESSES OF THE SWITCHES

The AC-DC converter shown in *Fig. 1a* when operated from a positive half-cycle of sinusoidal ac line voltage is well represented with a DC-DC converter shown in *Fig. 2a*. The corresponding converter models for ON-time interval (*Fig. 2b*) and for OFF-time interval (*Fig. 2c*) directly result in the voltage stresses of three switches as:

$$V_{CR1} = V_{CR2} = V_S = V \quad (1)$$

where V is the output DC voltage, since from *Fig. 2a:*

$$V_g + V_{Cr} = V \quad (2)$$

The relationship (1) is graphically shown on *Fig. 2d* as a straight line with relative gain of 1, to illustrate the important advantage of this topology that all three switches have for any operating duty ratio the same voltage stress equal to the output voltage V. This should be, for example, compared with the voltage stresses for the flyback converter. Although the flyback converter has two switches only, each of the switches has at 50% duty ratio the voltage stress equal to twice the output DC voltage.

Therefore, if the flyback converter were used for an AC-DC converter with V=400V output, it would need switches rated at 1200V, as opposed to 600V rated switches in the converter of *Fig. 1a*. However, the 1200V rated

switch (in this case, IXYS' IXTH12N1200 switch in a TO-247 package), exhibits 1.4Ω ON-resistance and 280pF drain-to-source capacitance. By comparison, the best-in-class 600V rated device in the same TO-247 package, the IPW66R037C6 from Infineon, exhibits a 37mΩ ON-resistance and 130pF drain-to-source capacitance.

Note that this configuration achieves almost a 40 times a reduction in ON-resistance and corresponding reduced conduction losses, and more than 2 times reduced drain-to-source capacitance for reduced switching losses as well. This clearly makes the flyback converter much less efficient than the new converter topology of *Fig. 1a*. When it is also recognized that the conventional flyback converter cannot be used without front-end bridge rectifier for AC-DC conversion, the efficiency gap becomes even much bigger.

DETAILED ANALYSIS

Operation from Positive Input Voltage

First, we analyze the operation of the converter in *Fig. 3a* in which the input voltage source is positive dc voltage and having the switch states as in *Fig. 3b*. The linear switched network for ON-time interval is shown in *Fig. 3c* and linear switched network for OFF-time interval is shown in *Fig. 3d*. To simplify the analysis, we will assume that the inductor L is very large, resulting in a constant input dc current I with negligible ac ripple current.

Flux Balance of Two Inductors and DC Voltage Gain

The Volt-second (flux balance) on inductor L requires that for the steady-state, the positive and negative areas of the voltage waveform in *Fig. 4a* must be equal so that:

$$V_g D T_S = V_{Cr} (1-D) T_S \qquad (3)$$

where:

V_g = input voltage
D = Duty ratio
T_s = Switching period in seconds

V_{Cr} = DC voltage on the resonant capacitor

Unlike the PWM inductor, L, which was flux balanced over the entire switching period Ts, the resonant inductor Lr must be fully flux balanced during the ON-time interval only as seen in *Fig. 4b*. Thus applying the steady-state criteria for the resonant inductor Lr in the loop consisting of Vg, Cr, Lr and V results in:

$$V_g + V_{Cr} - V = 0 \qquad (4)$$

as the resonant inductor must be flux-balanced and cannot support any net DC voltage.

Solving (3) and (4) results in;

$$V_{Cr} = V_g D / (1-D) \qquad (5)$$

$$V = V_g 1/ (1-D) \qquad (6)$$

Note that the dc conversion ratio given by Equation (6) is the same as for well-known boost converter. Furthermore, despite the resonant circuit consisting of resonant capacitor Cr and resonant inductor Lr, and corresponding sinusoidal and co-sinusoidal time domain waveforms of resonant current and resonant capacitor voltage, the dc conversion ratio does not depend on either one of them and their values or the switching period T_s, but only depends on the operating duty ratio, D, as in conventional PWM dc-dc converters. Hence, the regular duty ratio control can be employed to use this converter as a basis for PFC control as in boost and other conventional converters.

The resonant inductor current ir during entire switching period is shown in *Fig. 5a*, while the resonant capacitor voltage shown in *Fig. 5b* displays the linear charging of the resonant capacitor Cr during the OFF-time interval. Note also the continuity of the capacitor voltage at the transition between two switching intervals.

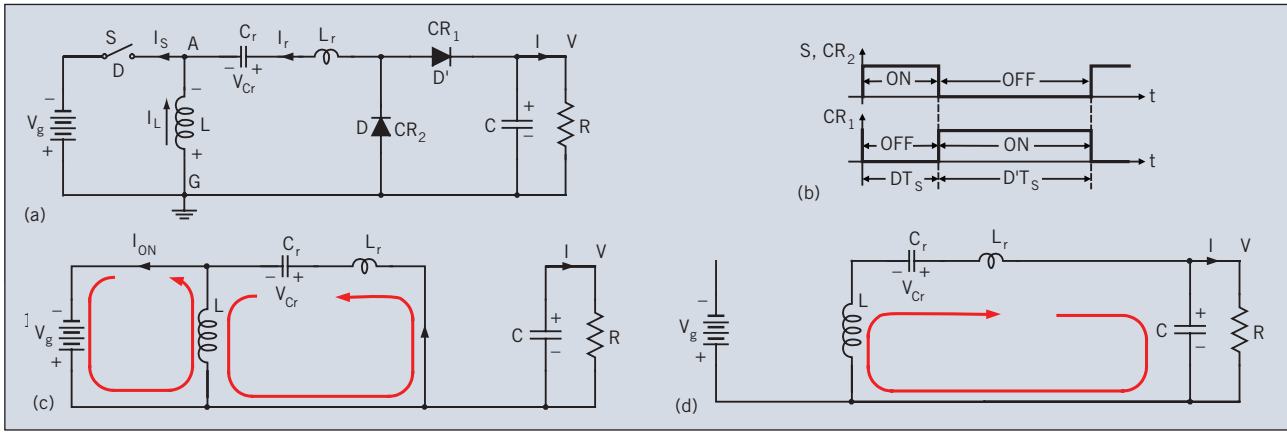

Fig. 6. Bridgeless PFC converter operation for negative half-cycle of input voltage: (a) Switch S operates in phase with diode CR2 and out of phase with diode CR1. (b) States of the switches of PFC converter (c) Linear switched networks for ON-time interval (d) Linear switched network for OFF-time interval

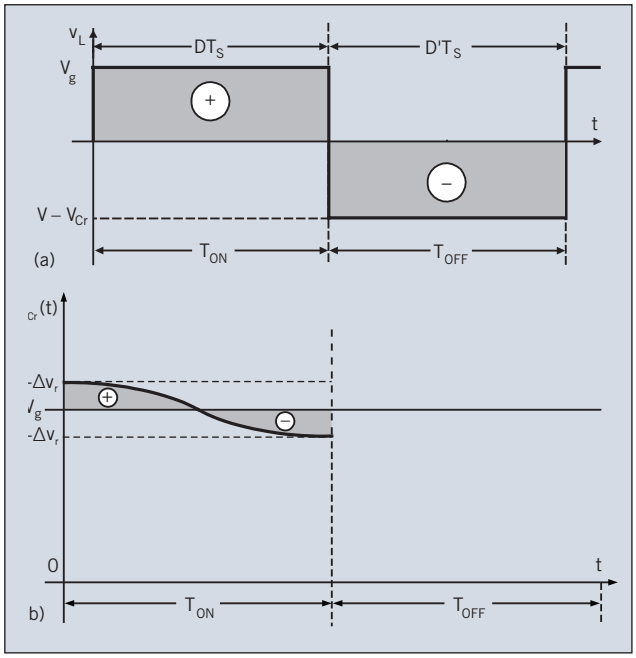

Fig. 7. PWM inductor L is excited as in PWM converters with a square-wave like voltage over entire switching period while resonant inductor Lr is excited over the ON-time interval only: (a) Voltage waveform of the PWM inductor and respective positive flux excursions (shaded area designated with positive sign) and negative flux excursion (shaded area designated with negative sign) (b) Resonant inductor Lr is excited with a co-sinusoidal ac ripple voltage Δvr of the resonant capacitor Cr and is fully flux-balanced during only ON-time interval (see respective shaded areas).

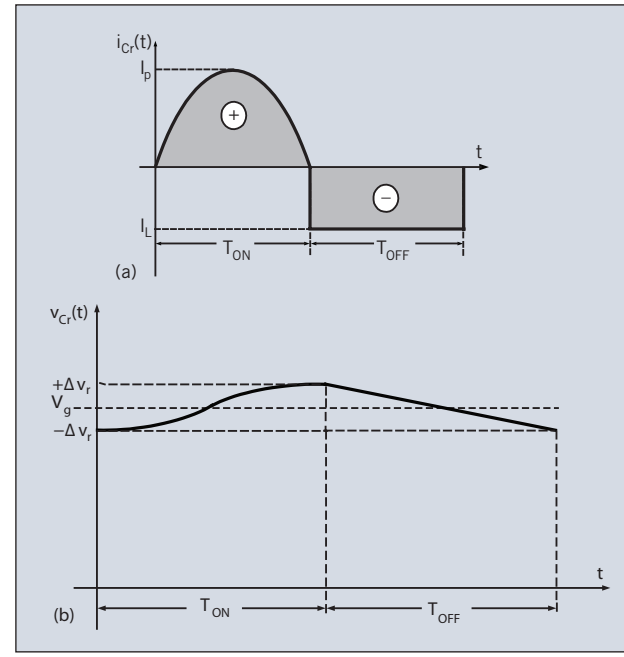

Fig. 8. Resonant inductor current and resonant capacitor voltage waveforms (a) Resonant inductor current ir during entire switching period (b) Resonant capacitor voltage shows the linear discharge of the resonant capacitor Cr during the OFF-time interval.

Operation from Negative Input Voltage

Next, we analyze the operation of the converter in *Fig.* 6a, in which the input voltage source is negative polarity dc voltage and having the switch states as in *Fig. 6b*. *Fig. 6c* shows the linear switched networks for ON-time interval, while *Fig. 6d* shows the linear switched network for the OFF-time interval.

Flux (Volt-second) Balance of Two Inductors and DC voltage Gain

We now use the two linear switched networks in *Fig. 6c* and *Fig. 6d* to construct the time domain of the current in the PWM inductor L and in the resonant inductor Lr. The voltage waveform on inductor L is shown in *Fig. 7a* to be just as in conventional PWM square-wave switching converters, while the resonant capacitor V_{cr} voltage is illustrated in *Fig. 7b* only for ON-time resonant interval and its complete time domain waveform in *Fig. 8b*.

The Volt-second (flux) balance on inductor L requires that for the steady-state, the positive and negative areas of the voltage waveforms in *Fig. 7a* must be equal so that:

$$V_g DT_S = (V - V_{Cr})\,(1-D)T_S \qquad (7)$$

Unlike the PWM inductor, which was flux balanced over the entire period T_s, the resonant inductor must be fully flux-balanced during the ON-time interval only as per converter model of *Fig. 6c*, in which the loop consisting of Vg, Cr, and Lr forms the resonant circuit model. From which:

$$Vg - V_{Cr} = 0 \qquad (8)$$

Solving (7) and (8) results in:

$$V_{Cr} = Vg \qquad (9)$$

$$V = Vg\ 1/\ (1\text{-}D) \qquad (10)$$

Therefore, despite different DC voltages on the resonant capacitor Cr for positive input voltage (D/ (1-D)) and for negative input voltage (input DC voltage Vg), the DC conversion ratios are identical for positive and negative polarity input voltages as shown by (6) and (10).

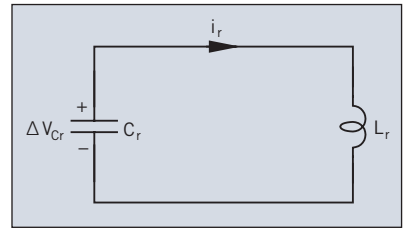

Fig. 9. Resonant circuit model for both positive and negative half-cycle of line voltage.

As before, the resonant current ir charging capacitor Cr is limited to only a positive cycle of resonant current as current rectifier CR2 now permits conduction in only one direction as in Fig. 8a. As the resonant current starts at zero level, this effectively restricts the reso-

nant charge interval once again to exactly one-half of the resonant period, the same as for positive input voltage.

The waveforms over the complete period for resonant inductor current ir(t) and resonant capacitor voltage vCr(t) are illustrated in *Fig. 8a* and *Fig. 8b*. Note how the continuity of the voltage on resonant capacitor results in the same ac ripple voltage Δvr at the transition between two intervals. Once again, the resonant capacitor dc voltage is now different and equal to dc input voltage Vg. Thus, the same dc voltage gain is obtained despite drastically different steady-state values of dc voltage on capacitor Cr The final resonant circuit model for both positive input voltage and for negative input voltage are identical and illustrated in *Fig. 9*.

RESONANT CIRCUIT ANALYSIS

As seen above, operation of the converter from positive input voltage and negative input voltage results in the same resonant circuit model, which results in the following solution:

$$i_r(t) = I_P \sin(\omega_r t) \qquad (11)$$

$$v_{Cr}(t) = \Delta v_r \cos(\omega_r t) \qquad (12)$$

$$\Delta v_r = I_P R_N \qquad (13)$$

$$R_N = \sqrt{L_r / C_r} \qquad (14)$$

$$\omega_r = 1/\sqrt{L_r C_r} \qquad (15)$$

$$f_r = \omega_r / (2\pi) \qquad (16)$$

where RN is the natural resistance, fr is the resonant frequency and ωr radial frequency.

The Bridgeless PFC converter of *Fig. 1a* has one controlling switch S. From the description of the converter operation for positive and negative output voltages, it is clear that this switch S must have a two-quadrant switching characteristic operating in the first and third quadrant as illustrated in *Fig. 10a*. In other words, switch S must for positive input voltage operate in first quadrant, but should also be able to sustain a full reverse voltage (third quadrant operation). Clearly, neither bipolar nor MOSFET transistors can do that as they are not designed to sustain voltage in the third

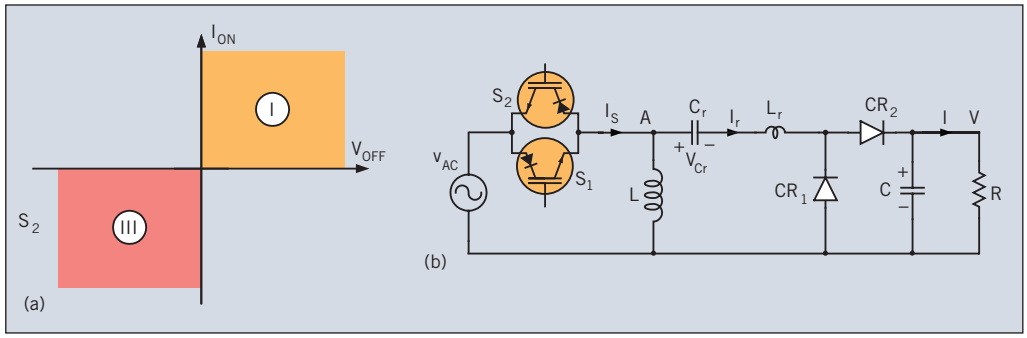

Fig. 10. Implementation of the controlling switch S. (a) Switch S must operate for positive input voltage polarity in first quadrant and sustain a full reverse voltage in the third quadrant. For negative polarity input voltage, the switch must operate in the third quadrant but still must be able to sustain a full reverse voltage in the first quadrant. (b) Implementation of switch S with two Reverse Blocking Isolated Gate Bipolar Transistors (RBIGBTs) connected in parallel.

quadrant (MOSFET due to presence of the body diode). However, the Reverse Blocking Isolated Gate Bipolar Transistor (RBIGBT) can sustain the full reverse voltage as it is designed to do so and can sustain the full voltage of opposing polarity. Therefore, the switch S implementation of *Fig. 10b* uses two such RBIGBT devices in parallel.

Yet, in many practical applications the MOSFET implementation is desired due to high switching frequency capability and low conduction losses. At present, a single MOSFET implementation is not possible due to built-in body-diode, so that switch S must be implemented by use of the two MOSFET devices connected back-to-back in series as shown in *Fig. 11a* by using two n-channel MOSFET devices, S1 and S2, connected at their sources and driven by a common floating gate drive circuit. Such an implementation results in full four-quadrant switch capability as shown in *Fig. 11b*, which is not required for converter operation as the two-quadrant of Fig. 10a is sufficient.

It is expected that a single first-third quadrant switch having the characteristics of *Fig. 10a* will be produced as a planar n-channel MOSFET in which two-quadrant operation comes naturally from the semiconductor device construction. This will dramatically reduce the conduction losses of the switch S by a factor of four times or more, since such two n-channel devices could be connected in parallel and not in series. As conduction losses are the converter's biggest losses by far, such a switch implementation could push the converter's efficiency over 98% in the near future.

The current direction in the resonant inductor is changing from one direction in OFF-time interval to another in ON-time interval. This short-duration change could cause the voltage spikes on the switch S - the faster the change, the larger the voltage spike. But due to small energy stored in this small inductor, this spike can be effectively suppressed by use of a Zener diode. Since the converter operates for both polarities of the input voltage, a bi-directional Zener diode, called Transorber, is used to dissipate all of the spike energy and limit the spike voltage. This, once again would dissipate all of the spike energy and limit the spike voltage. However, several non-dissipative ways also can be employed to recover most of the energy contained and deliver it to the load, thus increasing the efficiency and reducing switch stresses during the transition.

DC-DC CONVERTER CONTROL

Duty ratio control with constant switching frequency

We now describe one of the possible control methods of the dc-dc converter in *Fig. 3a* using the constant switching frequency and variable duty ratio control. The converter prototype was built to verify operation and record the characteristic waveforms for three operating duty ratios: D=0.5 (Fig. 12a), D= 0.66 (Fig. 12b) and D= 0.8 (Fig. 12c) resulting in output voltages of 18.1V, 28.6V, and 56V respectively, for the 10V input. The measurements were made at a constant 0.5A load current. The four traces show, from top to bottom: drain-to-source voltage of the controlling switch S, input source current, output load current and inductor L current.

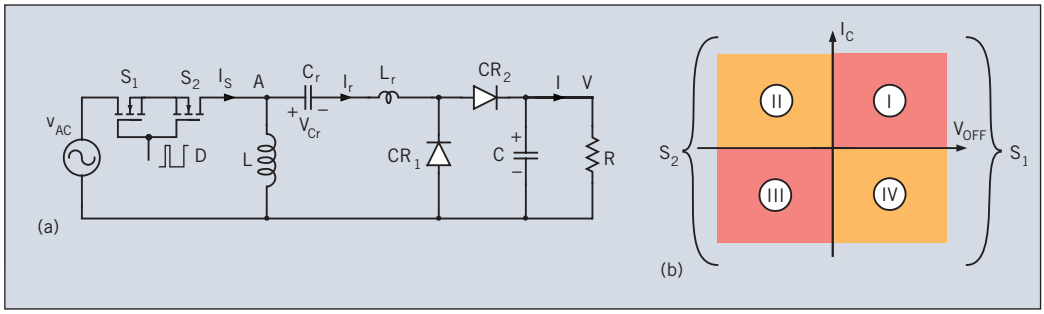

Fig. 11. Implementation of the controlling switch S. (a) Implementation of switch S with, two n-channel MOSFETs, S1 and S2, connected back-to-back at their sources and driven by a common floating gate drive circuit. (b) Switch S implementation with two MOSFETs operates in the four-quadrants.

Note how the input current (second trace) consists of the sum of

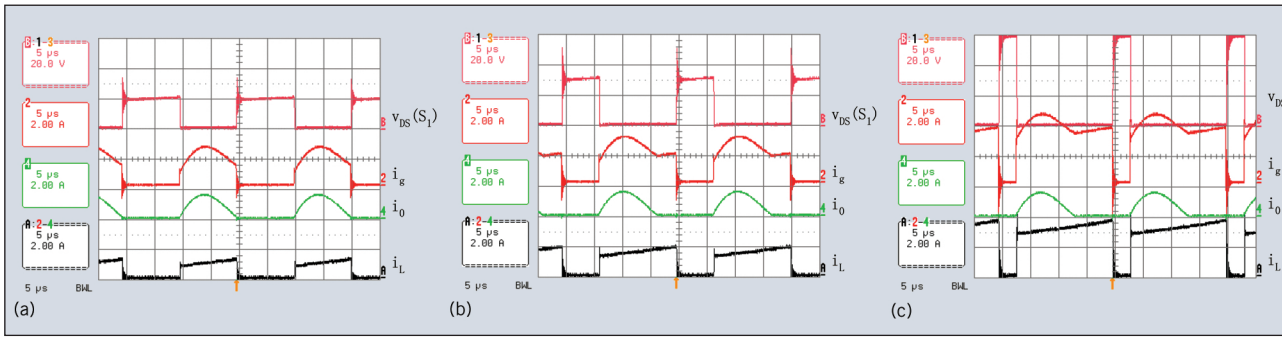

Fig. 12. Salient waveforms of the converter in Fig. 3a for constant switching frequency and variable duty ratio control a)for duty ratio D=0.5 b)for duty ratio D= 0.66 c)for duty ratio D= 0.8

resonant inductor Lr current (third trace) and inductor L current (fourth trace) thus confirming the fundamental relationships of the converter in *Fig. 3a*:

$$i_g = i_r + i_L \quad (17)$$

$$i_0 = i_r \quad (18)$$

Note also from (18) that the output current is identical to the resonant inductor current and therefore it has both the same shape and duration for all three operating cases and is therefore not changing, but has the same shape and magnitude as for 50% duty ratio. Therefore, the input current shape and magnitude are changing so that the DC current conversion ratio is changed, which ultimately results in corresponding change in the DC voltage conversion ratios. This is qualitatively different from the conventional boost converter operation, in which the high duty ratios result in shorter duration of the pulse delivery of the load current (at 0.9 duty ratio it would be 10% of the period). In this example, the delivery of the load current is always at 50% of the constant switching period.

In this case, the resonant interval is designed to coincide with the 50% duty ratio so that the time variation of the inductor L current at that operating point is hidden and not explicitly seen (*Fig. 12a*) as it is in the waveforms of *Fig. 12b* and *Fig. 12c* for duty ratios higher than 50%.

Constant ON-time-interval and variable OFF-time interval control

The converter prototype is then operated with constant ON-time and variable OFF-time control and the characteristic waveforms for three effective operating duty ratios are recorded: D=0.5 (*Fig. 13a*), D= 0.66 (*Fig. 13b*) and D= 0.8 (*Fig. 13c*) resulting in output voltages of 19.3V, 28.8V and 45V, respectively for the 10V input voltage. The measurements were made at a constant 0.5A load current. The four traces show from top to bottom: drain-to-source voltage of the controlling switch S, input source current, output load current and inductor L current.

Note how for higher duty ratios, both input current and output current are conducting for almost the entire interval, resulting in quasi-continuous input and output currents. The output current also has reduced peak values of the resonant currents and will require minimum output capacitance to filter this nearly continuous output current.

TWO DC-DC CONVERTERS IN ONE

Voltage gains (6) and (10) derived so far are really representing dc voltage gain only for the converter in *Fig. 3a* for the

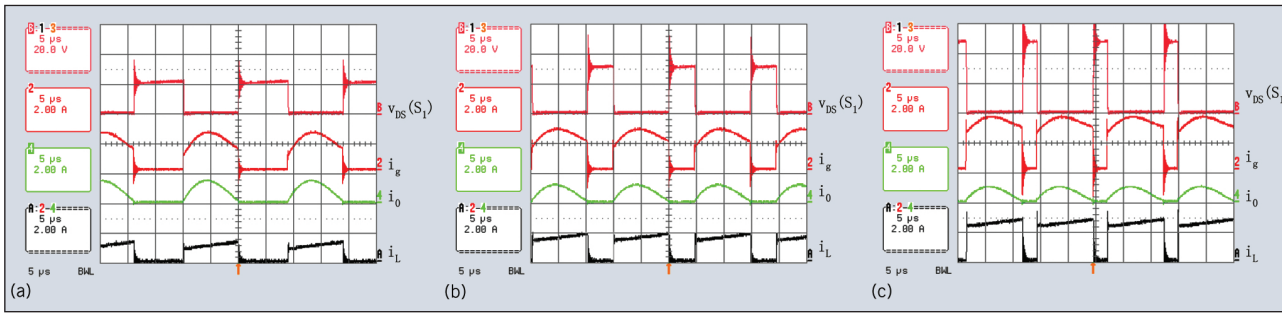

Fig. 13. Characteristic waveforms for converters in Fig. 3a for variable off-time and for three effective operating duty ratios a) D=0.5, b) D= 0.66 c) D= 0.8

duty ratios D higher than the resonant duty ratio DR that is :

$$V/Vg = 1/(1-D) \text{ for } D > D_R \quad (19)$$

$$D_R = T_R / 2T_S \quad (20)$$

$$T_R = 1/fr \quad (21)$$

and (20 and (21) are definitions of the two quantities DR and T_R. The voltage conversion ratio for duty ratios lower than D_R can be evaluated using the extension of the State-Space Averaging Method (1,2) introduced in (3) is outside of the scope of this article. Nevertheless, the following analytical results is obtained:

$$V/Vg = D/(1-D)\, D_R \text{ for } D < D_R \quad (22)$$

Note how the DC voltage gain (22) for D=DR changes into formula for DC conversion given by (19). As DR is simply a design constant, the overall dc voltage gain of the converter in *Fig. 3a* changes form the step-down/step-up conversion given by (22) for low duty ratios to step-up only voltage gain given by (19) for higher duty ratios with a continuous smooth transition at duty ratio DR. This results in two converters in one, as shown in the composite voltage gain in *Fig. 14*.

Therefore the dc-dc converter of *Fig. 3a* solves two problems which were plaguing conventional boost and buck-boost converters:

a) boost converter due to its boost voltage gain 1/(1-D) in its non-isolated version did not have a soft start, and just the opposite had a high in-rush input current so that additional circuit needed to be employed to reduce in-rush currents. In the isolated case, separate circuitry is needed to charge the capacitor on the output to the input voltage so that the converter could be started.

b) buck-boost (flyback) converter has a step-down/step-up dc voltage gain so that a soft start is provided without any additional circuitry for both non-isolated and isolated versions. On the other hand, as shown earlier, the buck-boost converter causes very high voltage stresses on its two switching devices several times that of the output DC voltage.

The dc converter of *Fig. 3a*, however, combines the best features of both boost and flyback converters and simultaneously eliminates their bad properties such that:

a) voltage stresses of all switches are equal to output dc voltage under all operating conditions

b) soft-start is provided with voltage dc gain having characteristic of step-down/step-up dc voltage gain in the low duty ration region.

It is easy to verify that the above properties are also present in the dc-dc converter with the negative dc input voltage, so that the above advantages will be also present if the bridgeless ac-dc converters of *Fig. 1a* and *Fig. 1b*. These converters also allow operation directly of the ac line and eliminate the bridge rectifier, unlike conventional boost and flyback converters.

PFC Conversion Function

The equality of the dc conversion gains as a function of duty ratio D of the controlling switch S proven above is one important pre-requisite for a converter to operate as a Single-Stage ac-dc (Bridgeless) converter with PFC function.

Another factor is that both DC conversion gains are having a step-up dc gain characteristic which is another pre-requisite needed for the converter topology to qualify as Single-Stage ac-dc (Bridgeless) converter topology. This therefore establishes that the converter of *Fig. 1b* is able to operate as a single-stage (bridgeless) ac-dc PFC converter.

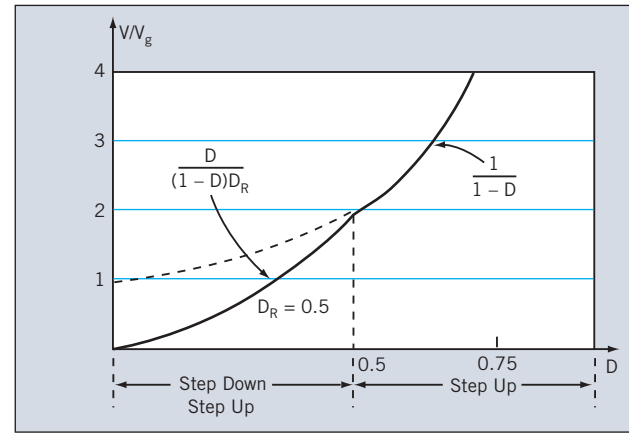

Fig. 14. Start-up operation. Theoretical dc conversion gain characteristic shown exhibits the step-down/step-up voltage gain characteristic at low duty ratios and transforms itself into a step-up only dc voltage gain characteristic at duty ratio D_R.

In a departure from previous attempts at bridgeless PFC conversion, all three switches, inductor L, resonant inductor Lr, and resonant capacitor Cr are 100% utilized as they take part in PFC operation for both positive as well as negative part of input line ac voltage.

The Power Factor Correction is based on controlling the average input current of the converters in *Fig. 1b* to become proportional and in phase to the input ac line voltage by use of the Bridgeless PFC IC controller. Thus, the duty ratio modulation is used to control average input current of the ac-dc switching converter of *Fig. 1b*, since it was demonstrated that such a duty ratio control is effective in controlling the converter for either positive or negative parts of the ac line voltage. The PFC control operates in two modes :

1.Duty ratio modulation with constant switching frequency.

2. Constant ON-time and variable OFF time and therefore, variable switching frequency.

LOOKING AHEAD

The fourth in a series of "impossible" converter solutions, The Bi-directional Isolated Step-up Converter, will be introduced in the January 2011 issue of Power Electronics Technology. This converter, shown in *Fig. 15*, comprises three MOSFET switches and two magnetic components. It has a bi-directional power flow capability to convert input low battery voltage VL (14V-32V) to high output battery voltage VH (270V) and vice versa.

Editorial Note: For questions regarding this article and for contact information to the author the readers are directed to TESLAcoís Web site www.teslaco.com.

Footnote: Isolated Bridgeless PFC Converter™ and Single-Stage Isolated PFC Converter™ are trademarks of TESLAco.

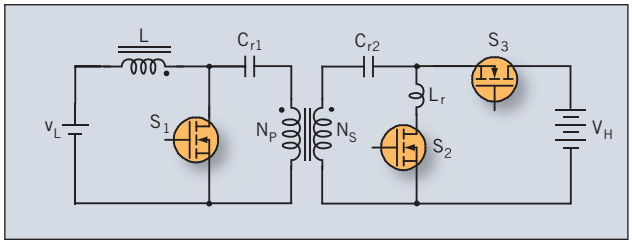

Fig. 15. The fourth "impossible" converter solution, an Isolated Step-up dc-dc Converter with Bi-directional current flow capability uses only three MOSFET switches, and two magnetic parts, in addition to a small resonant inductor and small resonant capacitor.

REFERENCES

1. Slobodan Cuk, "Modelling, Analysis and Design of Switching Converters", PhD thesis, November 1976, California Institute of Technology, Pasadena, California, USA.

2. Slobodan Cuk, R.D. Middlebrook, "Advances in Switched-Mode Power Conversion", Vol. 1, II, and III, TESLAco 1981 and 1983.

3. Slobodan Cuk, "State-Space Averaging: Past, Present and Future". Invited paper, APEC Power Electronics Conference, Fort Worth, Texas, March 6, 2011.